JOURNAL OF MATERIALS SCIENCE **36** (2001) 4625–4631

Elevated temperature ablation resistance and thermophysical properties of tungsten matrix composites reinforced with ZrC particles

G. M. SONG
School of Materials Science and Engineering, P O Box 433, Harbin Institute of Technology, Harbin 150001, People's Republic of China; Institute of Engineering Mechanics, Harbin 150080, People's Republic of China
E-mail: songguim@hotmail.com

Y. J. WANG, Y. ZHOU
School of Materials Science and Engineering, P O Box 433, Harbin Institute of Technology, Harbin 150001, People's Republic of China

In order to improve the elevated temperature ablation resistance of the copper infiltrated tungsten materials (Cu/W) which are used as the rudders of the rocket motors at present, a new kind of tungsten matrix composites reinforced by 30 vol% zirconium carbide particles (ZrC_p/W) was developed, and the elevated temperature ablation resistance and thermophysical properties of the new materials were investigated. The values of the mass ablation rate and linear ablation rate of ZrC_p/W were much lower than that of Cu/W, which indicated that the addition of ZrC particles in tungsten matrix remarkably increased the ablation resistance. Thermal thermochemical oxidation of tungsten and ZrC particles was the main ablation mechanism of ZrC_p/W. A self-made dynamic responding multi-wavelength pyrometer was employed to measure the ablated surface temperatures and a thermal couple was employed to measure the back surface temperatures. The important temperature curves of the ablated surface and back surface of the specimens were successfully detected online, which indicated that ZrC_p/W has good thermal shock resistance. The present of ZrC particles in tungsten matrix remarkably decreased the thermal conductivity and thermal diffusivity of the ZrC_p/W composites, which is very useful for increasing the elevated temperature ablation resistance of the composites. The excellent elevated temperature ablation resistance of ZrC_p/W is attributed to the lower thermal conductivity, lower thermal diffusivity, oxidation resistance and high melting points. The good properties of ZrC_p/W makes it be suitable for the rudders for rocket motors instead of Cu/W.

1. Introduction

Copper infiltrated tungsten material (Cu/W) is usually used in high temperature environment for its high strength at elevated temperature, high thermal shock resistance and high ablation resistance [1, 2]. At present, Cu/W is used as these rudders for rocket motors. But the ablation resistance of the rudder needs to be much improved in order to keep its good pneumatic shape when the working time is long (for example, more than 120 s) [3].

The work temperature of a rudder of a rocket motor is usually above 2000°C. At the retrofire time of a rocket motor, the rudder temperature is increased drastically from room temperature to above 2000°C during a second [4, 5]. The abominable work environment of the rudders makes it be a formidable task to improve remarkably the elevated temperature ablation resistance of Cu/W [1]. Composite materials give us the advantage of designing the mechanical and/or physical and/or chemical properties of the composites by changing the compositions or phases contents or preparation techniques [6, 7]. The authors have already reported the idea of materials design and microstructure control to prepare composites with high performances [8, 9]. ZrC possesses high melting point, 3530°C, high ablation resistance, lower thermal conductivity compared with tungsten [10]. In addition, ZrC is compatible with tungsten [11]. The addition of ZrC particles in tungsten matrix should improve the ablation resistance of tungsten. In this paper, we try to develop a new kind of tungsten matrix composites with good elevated temperature ablation resistance and good thermophysical properties which are suitable for the rudders for the rocket motors instead of Cu/W.

2. Experimental

2.1. Materials fabrication

99.9 wt% tungsten powders with a mean size of 3.5 μm and 98 wt% ZrC particles with a mean size of 2.5 μm were used as starting materials of ZrC_p/W. W and ZrC were mixed in ratio of 70 : 30 vol. for 24 h. The resulting powder mixtures were then cold formed in a steel mould, and then hot pressed in a graphite mould at 2000°C under a vacuum of 1.3×10^{-3} Pa for 1 h with an applied pressure of 20 MPa. Pure tungsten material was prepared using the same method as ZrC_p/W. For comparison with the ZrC_p/W, Cu/W (the copper content is ~20 vol%) were prepared. A porous tungsten skeleton was sintered at 2250° in a hydrogen atmosphere for 5 h to a controlled porosity level. This skeleton was subsequently infiltrated with molten copper at 1350°C in hydrogen for 2 h.

2.2. Ablation facility

The main test facilities for ablation property of the rudder are rocket motors, but the experiments are very costly. The simulation ablation tests on the ground are usually used in order to reduce the cost and give out a primary evaluation of the materials. Oxyacetylene ablation as a kind of simulation ablation method is extensively used in our country due to its low cost and easy operation. In this study, an oxyacetylene ablation facility including an ablation system and a set of temperatures detect system (see Fig. 1) was self-made according to GJB323A-96 Ablation Standard of China. The ablation system includes a specimen holder made of graphite and an oxyacetylene gun, and the detecting system includes a dynamic responding multi-wavelength pyrometer used for measuring the ablation surface temperature and a thermal couple employed to measure the back surface temperature during eroding. Fig. 2 shows a specimen fixed in the graphite holder. The wavelength range of the pyrometer is 0.55–1.05 μm, therefore, C_2H_2, O_2, H_2O, H^+ and OH^- cannot effectively interfere in the signals of the ablated surface

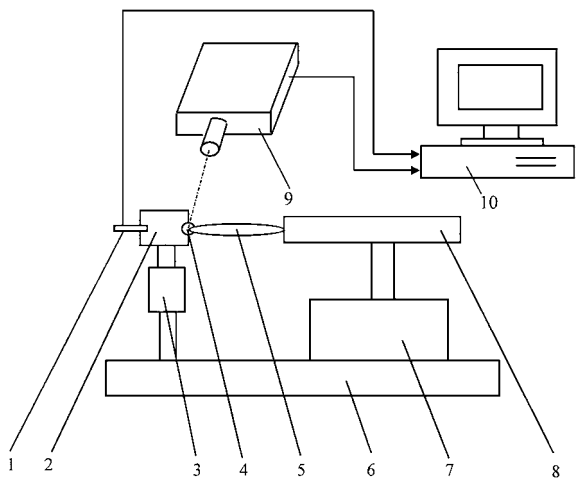

Figure 1 Schematic of the ablation facility. 1-thermal couple on the back of the specimen, 2-fixture for specimen, 3-rotating device, 4-ablating specimen, 5-oxyacetylene flame, 6-support structure, 7-steering unit for ablating gun, 8-oxyacetylene gun, 9-computer, 10-multi-wavelength pyrometer.

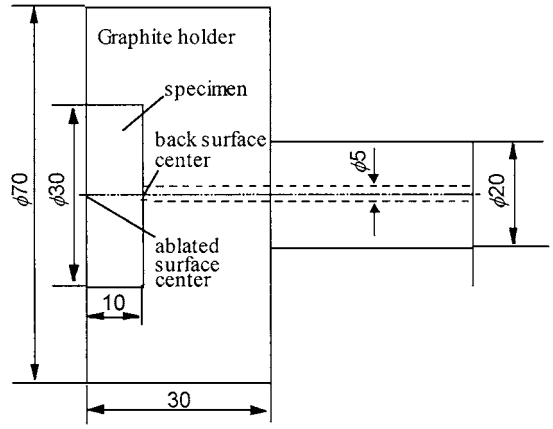

Figure 2 A specimen is fixed in a graphite holder.

temperatures detected by the pyrometer [12]. Furthermore, the millisecond-resolution system is possible to measure rapidly the specimen's temperature during an extremely short time, even though the chemical reactions or physical changes are very rapid. Data corresponding to temperatures are recorded and processed with a 80486 computer nominally every one millisecond with a signal resolution of about 0.5% in 800–1700°C and a signal resolution of about 1% in 1700–3500°C. The dynamic techniques can detect online the ablated surface temperatures of the specimens during heating and cooling and display the temperature-time curves at the same time on the computer screen.

2.3. Ablation testing

The specimens with dimensions of $\phi 30 \times 10\,\text{mm}^3$ were used for mass ablation rates and linear ablation rates measurements. The tests were conducted according to GJB322A-96 Standard on the oxyacetylene facility. The press and the flux of acetylene were 0.095 MPa and 1.116 m^3/h, respectively. The press and the flux of oxygen were 0.4 MPa and 1.512 m^3/h, respectively.

The mass ablation rate, R_m, is defined as:

$$R_m = \frac{m_1 - m_2}{t} \tag{1}$$

where m_1 and m_2 are the mass before and after ablation, respectively, and t being the ablation time.

The linear ablation rate, R_d, is defined as:

$$R_d = \frac{d_1 - d_2}{t} \tag{2}$$

d_1 and d_2 here represent the thickness before and after ablation, respectively, and t being the ablation time.

The microstructure of the ablated surface and vertical section of the specimens were studied by scanning electron microscopy (SEM) and X-ray diffraction (XRD).

2.4. Thermophysical properties testing

Measurements of thermal diffusivity, a, of the composites were carried out by using a laser flash method. The sizes of the specimens are $\phi 10 \times 1.2$–$2\,\text{mm}^3$. a can be

calculated by the following equation [13]

$$a = \frac{0.139L}{t_{1/2}} \tag{3}$$

where L is the sample thickness, $t_{1/2}$ is the time required for the back surface of the sample to reach half of the maximum temperature rise (T_{max}), and 0.139 being a constant when heat loss is negligible and $t_{1/2}$ is much larger than the pulse duration of the laser. Then the thermal conductivity, λ, is obtained using the formula:

$$\lambda = aC_p\rho \tag{4}$$

where C_p is the specific heat at constant pressure and ρ is the density [14].

The C_p parameter was measured in a specific heat calorimeter, the temperature used was from 20°C to 1000°C and the specimen size is $\phi 10 \times 30$ mm^3. The density measured by Archimedes method at room temperature will by corrected by the thermal expansion results at various temperatures. Thermal expansion was measured from 20°C to 1000°C with a commercial thermomechanical analyzer. The specimen size was $3 \times 4 \times 10$ mm^3.

3. Results and discussion

3.1. Surface temperatures of the ablated specimens

Fig. 3 gives the temperature curves of ZrC_p/W, pure W and Cu/W specimens. The results show that the temperature rising velocity of the ablated surface of ZrC_p/W is the fastest among the three kinds of materials during the initial heating stage. In contrast, the temperature rising velocity of the back surface of ZrC_p/W is the slowest. During the initial stage (0–5 s), the temperatures rose fast, and the temperature changing trend was severely affected by the original temperature field of the specimen. As time passed (>5 s), the influence of the original temperature field gradually disappeared, and the further change of the temperatures of the specimen was depended on a heating discipline [15].

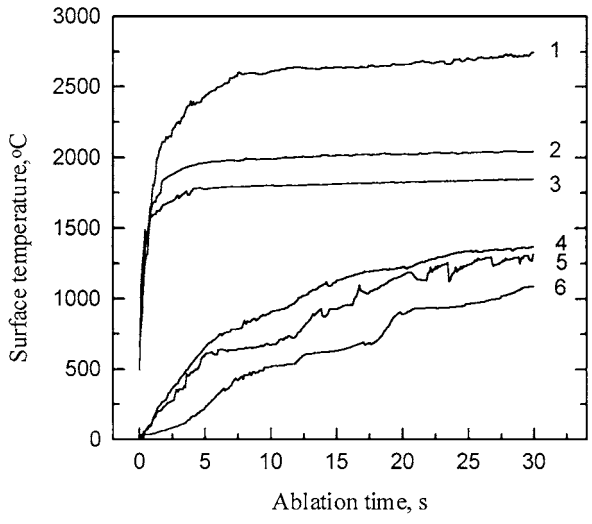

Figure 3 Temperature curves of ablated surface and back surface of the ablated specimens. 1, 2, 3–temperature curves of ablated surface center of ZrC_p/W, pure W and Cu/W, respectively; 4, 5, 6–temperature curves of back surface center of Cu/W, pure W and ZrC_p/W, respectively.

At the first second of heating, the ablated surface temperatures of ZrC_p/W specimen was 1988°C, implying that the temperature rising velocity was 2000°C/s or so during the first second of heating. The temperature variation rate of the ablated surface of ZrC_p/W caused by the oxyacetylene flame approaches that of the rudder at the retrofire time of rocket motors. In this paper, the dynamic surface temperature curves of the specimens were successfully detected online using the multi-wavelength pyrometer, which were very important for analyzing of elevated temperature ablation mechanisms and thermal shock behavior of the materials.

3.2. Ablation properties

Figs 4 and 5 show the ablation properties of the ZrC_p/W, pure W and Cu/W. The mass ablation rate and linear ablation rate of Cu/W during the initial 30 s were 92.4 mg/s and 13.8 μm/s, respectively, and those of ZrC_p/W were 13.1 mg/s and 3.71 μm/s, respectively. The ablation rate decreased as ablation time passed. The ablation zone became thicker with prolonging ablation time, which hindering the heat transferring from the

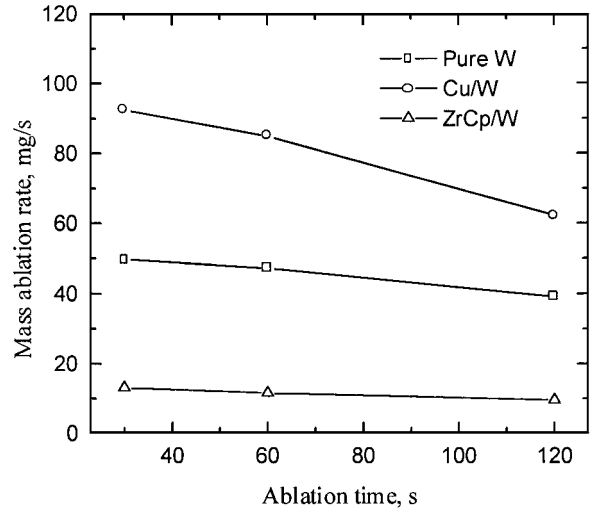

Figure 4 Mass ablation rates of ZrC_p/W, pure W and Cu/W.

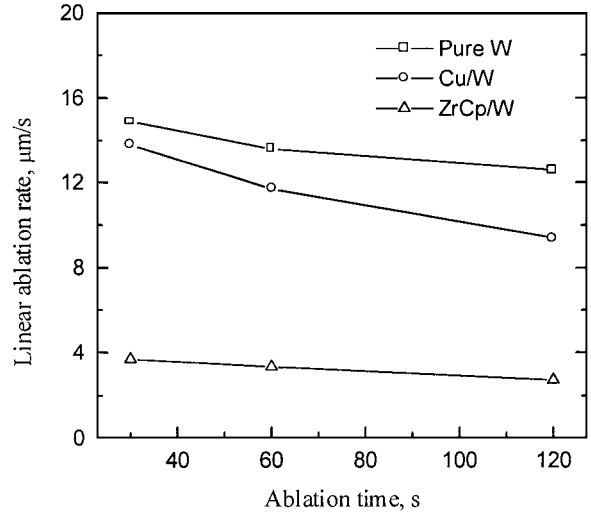

Figure 5 Linear ablation rates of ZrC_p/W, pure W and Cu/W.

outer into the inner, and the oxidation surface also hindered the further oxidation of the inner microstructure. The addition of ZrC particles remarkably increased the ablation resistance of the composites. The values of the mass ablation rate were in the order from high to low: Cu/W > pure W > ZrC_p/W, and the values of the linear ablation rate were in the order: pure W > Cu/W > ZrC_p/W. Due to the copper expelled from the tungsten skeleton for Cu/W during eroding, the mass loss of Cu/W is more than that of pure W and ZrC_p/W.

3.3. Ablated microstructure

Fig. 6a is a typical micrograph of ZrC_p/W showing a uniform distribution of ZrC particles throughout the tungsten matrix. The uniformity of the microstructure is believed to be responsible for the isotropic nature of the mechanical and thermophysical properties of ZrC_p/W. Fig. 6b is a macrograph of ablated ZrC_p/W specimen showing an oxidation layer of the ablated surface, which was identified by XRD as a mixture of tungstenic and zirconic oxides. The ablated surface was severely bubbled. Microstructure investigation showed

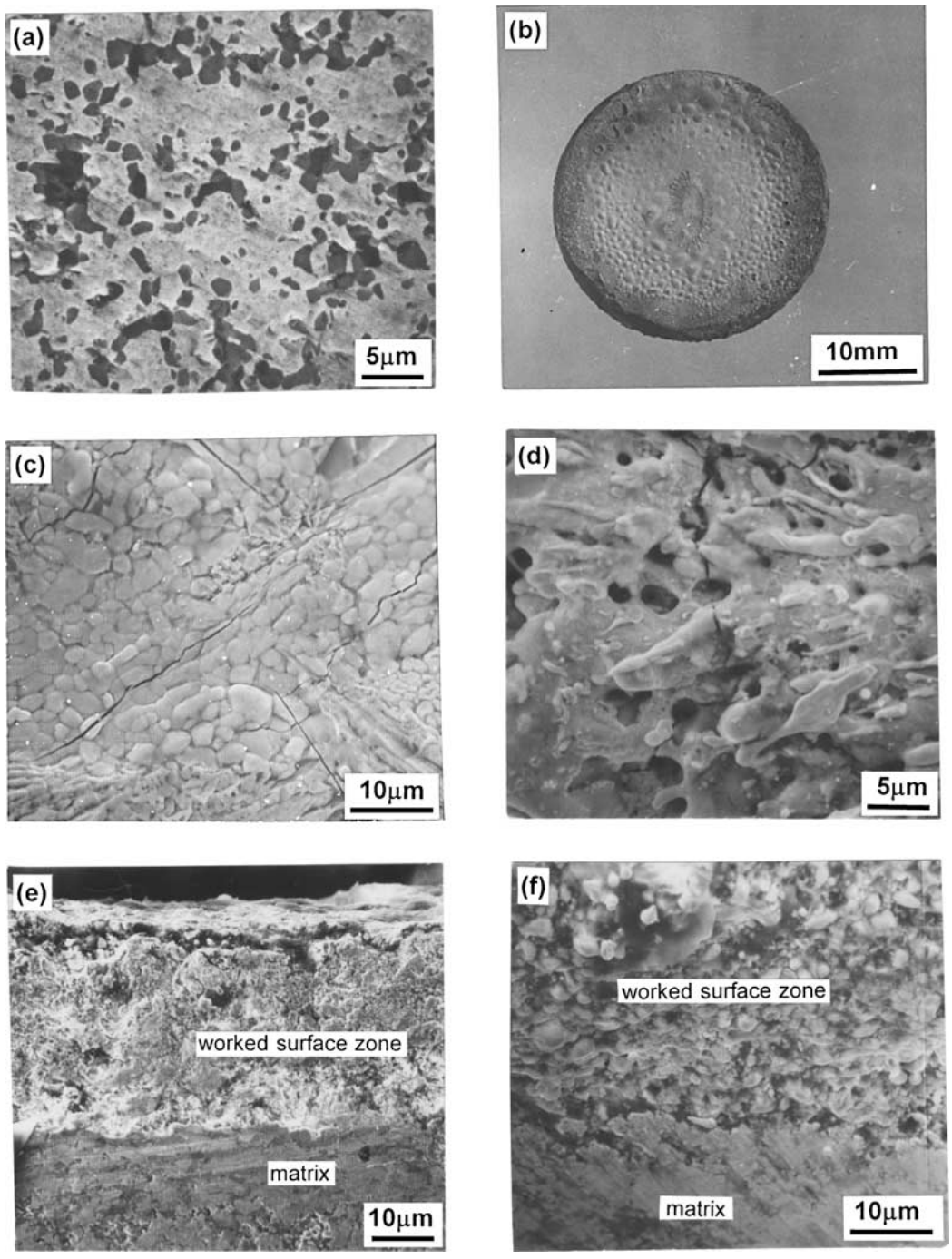

Figure 6 Morphologies of the ablated ZrC_p/W. (a) the secondry electron image of the of the polished surface of ZrC_p/W showing a uniform distribution of ZrC particles in tungsten matrix, (b) macro morphology of ablated surface of the specimen, (c) micro morphology of ablated surface showing microcracks, (d) micrograph of the river pattern showing a mechanical scour resulted from the airflow blowing, (e) A verticle section of the ablated surface showing a worked surface zone with a thickness of 30 μm, (f) micrograph of the worked surface zone showing a loose and porous microstructure.

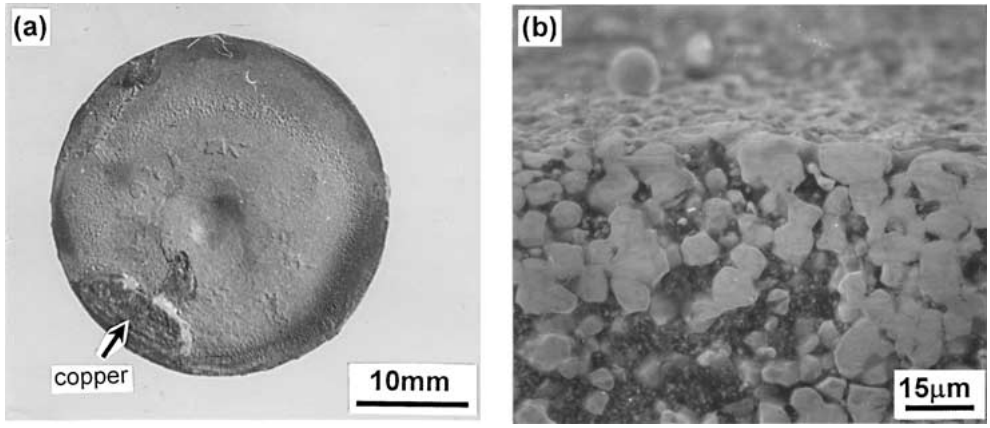

Figure 7 Ablated morphologies of Cu/W, (a) macrograph of ablated surface, showing a ablated crater and transudatory copper solidified on the ablated surface; (b) micrograph of the verticle section, showing atungsten skeleton where the copper expelled from the skeleton.

that there were many microcracks existed on the ablated surface, and majorities of them were straighter and connected to a net, and some oxidation layer peeled off (see Fig. 6c), but no macrocrack was observed in the sample. In the center zone of the ablated surface, the river pattern shows a mechanical scour resulted from the airflow blowing (Fig. 6b). Fig. 6d gives a micrograph of the river pattern. Vertical sections were also observed to examine changes in the surface zone of the specimen which was ablated for 120 s. The micrograph indicated that the thickness of the worked surface zone was about 25 μm (see Fig. 6e). Fig. 6f shows that the worked surface zone was loose due to the oxidation and scour effects of the airflow on the microstructure, and cracks were few and far between in the zone, implying that the microcracks in the ablated surface did not propagate into the matrix of the composites.

Fig. 7a shows the macro morphology of ablated surface of Cu/W. A lot of copper expelled from the tungsten skeleton and solidified on the ablated surface. From the vertical section of the ablated surface zone, a tungsten skeleton can be observed where the copper was expelled from the skeleton (see Fig. 7b).

3.4. Thermophysical properties

The values of thermal diffusivity, a, and thermal conductivity, λ, of pure W, ZrC_p/W and Cu/W in 20–1000°C were given out in Figs 8 and 9, respectively. Due to the low melting point of copper, 1083°C, the values of a and λ of the three kinds of materials above 1000°C were not examined. The thermal diffusivity of ZrC_p/W is about 28% of that of Cu/W at the same temperature, and the same as the thermal conductivity of ZrC_p/W. The addition of ZrC particles in the W matrix greatly decreased the values of a and λ of the composites. In contrast, Cu added into W matrix slightly increased the values of a and λ of the Cu/W due to the better thermal conductivity and better thermal diffusivity of copper compared with W [10].

3.5. Ablation mechanisms

During eroding, there were severe reactions between the oxidative gases (the ratio of the fluxes of oxygen and acetylene was O_2/C_3H_2=1.35/1) [16] and ZrC_p/W

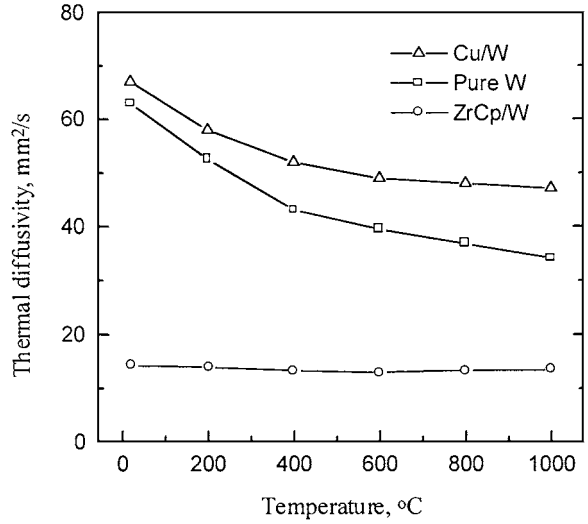

Figure 8 Thermal diffusivity of pure W, ZrC_p/W and Cu/W versus temperature.

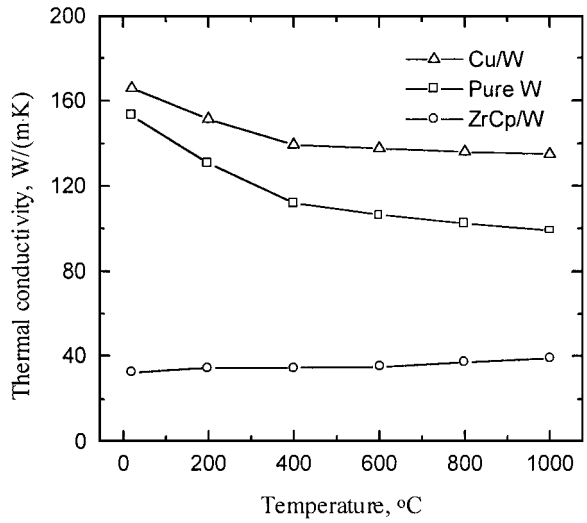

Figure 9 Thermal conductivity of pure W, ZrC_p/W and Cu/W versus temperature.

which were summarized by the following equations:

$$W + O_2 \rightarrow WO_3 \quad (5)$$

$$W + H_2O \rightarrow WO_3 + H_2 \quad (6)$$

$$W + CO_2 \rightarrow WO_3 + CO \quad (7)$$

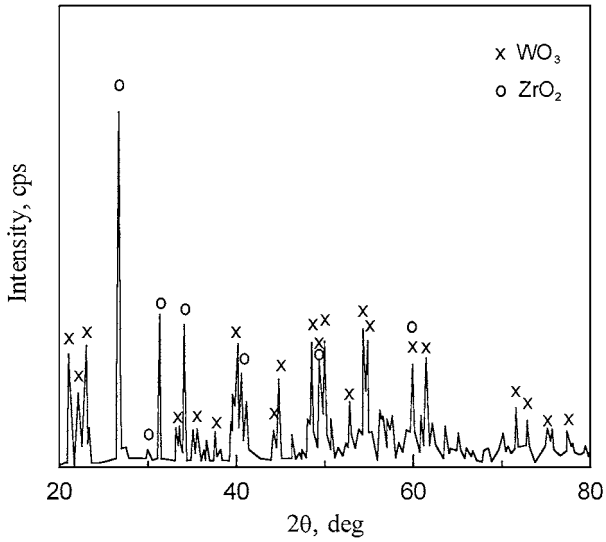

Figure 10 XRD pattern of the ablated surface of ZrC_p/W.

In fact, there were some transition oxides in the above reactions, such as WO_2, $WO_{2.72}$ and $WO_{2.90}$.

ZrC particles reacted with O_2:

$$ZrC + O_2 \rightarrow ZrO_2 + CO \tag{8}$$

ZrC particles also reacted with CO_2, but the reactions were minor

$$ZrC + CO_2 \rightarrow ZrO_2 + CO \tag{9}$$

The oxide phases of the ablated surface of ZrC_p/W were identified by XRD as ZrO_2 and WO_3 (see Fig. 10), showing that the tungsten and ZrC particles in the ablated surface were completely oxidized. The coefficient of thermal expansion of ZrO_2 is 10.8×10^{-6}/K, much higher than that of tungsten (4.5×10^{-6}/K). Furthermore, the transformation of ZrO_2 during heating and cooling caused a volume mutation [10]. Thereby the oxide layers were prone to bubble and peel, and they were also prone to be blown away by the high speed burning gases. There was a river pattern in the center zone of the ablated surface (see Fig. 6b), indicating the ablation resulted from the burning gases.

The ablation surface temperatures of ZrC_p/W specimens were about 2600–2700°C from the measured results (see Fig. 3), which was close to the melting points of ZrO_2 (~2680°C) and much lower than melting points of ZrC and tungsten, implying that ZrO_2 would melt during eroding [10]. Although the flame temperature could reach 3500°C, the heat transferring from the flame to the specimen's surfaces would consume time, which causes the surface temperature is lower than the flame temperature. Therefore the melting of W matrix and ZrC particles did not take place, and thermochemical oxidation of W matrix and ZrC particles is the main ablation mechanism of ZrC_p/W.

The oxidation resistance of tungsten is bad. Tungsten can react with oxygen at 400°C, and the final oxide is WO_3 with a yellow color [17]. WO_3 is loose and porous, and its melting point is 1470°C. WO_3 can sublime significantly at 850°C at 1 atmosphere [17]. During eroding, WO_3 would become a liquid film covered the ablated surface of the specimen when its sublimation was restrained at the press of the highspeed airflow, and then the liquid film were blown away by the airflow. The loose and porous WO_3 layer could not effectively separate the W matrix from oxidative gases. In contrast, the ZrO_2 layer of ZrC was compact, and could effectively protect the ZrC. Furthermore, when melted ZrO_2 covered the ablated surfaces, the ZrO_2 layer could hinder the oxidation of tungsten. As a result, the ablation resistance of the composite was increased significantly with an addition of ZrC particles.

For an isotropic material without any inner heat, the thermal diffusion equation in a cylindrical coordinate system is [15]

$$a\left(\frac{\partial^2 T}{\partial z^2} + \frac{\partial^2 T}{\partial y^2} + \frac{1}{r}\frac{\partial T}{\partial r}\right) = \frac{\partial T}{\partial t} \tag{10}$$

where, a is thermal diffusivity of the material, t and T are time and temperature, respectively. The heat transferring is fast if the thermal diffusivity is high during heating, which results in a lower temperature gradient in the specimen. The thermal diffusivity of pure W, ZrC_p/W and Cu/W at 20°C are 62.9 mm^2/s, 14.3 mm^2/s and 66.1 mm^2/s, respectively, thereby both of the ablated surface temperature and the temperature gradient in ZrC_p/W specimen are all the highest among the three kinds of materials during heating. In addition, the copper is melted, vaporized and expelled from the tungsten skeleton. The cooling effect of the copper serves to keep the temperature of Cu/W at a lower level. Due to the different thermophysical properties of these materials, the temperatures of ablated surface and back surface among various specimens were different under the same eroding condition (the same flame temperature).

Compared with pure W, Cu/W has higher mass ablation rate and lower linear rate. Copper expelled resulted in a higher mass ablation rate, whereas also resulted in a lower ablated surface temperature, which made the linear ablation rate be lower. The thermal conductivity of ZrC_p/W is much lower than that of Cu/W, and therefore, it is more difficult for the outer heating diffusing into the inner of the material. Furthermore, ZrO_2 is inorganic materials with a very lower thermal conductivity (~2.3 W/(m · K)), the oxidation layer can effectively prevent outer heating from diffusing into the inner of the specimens, and thus makes the high temperature zone locate in the surface layer. Due to the low thermal conductivity of ZrC_p/W and ZrO_2 oxidation layer compared with Cu/W, the ablation resistance of ZrC_p/W was greatly improved.

The elevated temperature ablation properties and thermophysical properties of pure W, ZrC_p/W and Cu/W are given out in Table I. ZrC_p/W possess better properties than Cu/W as we designed before. The ablation resistance mainly depends on the thermal conductivity, thermal diffusivity, oxidation resistance and melting points of the materials. The higher ablation

TABLE I Ablation properties and thermophysical properties of pure W, ZrC_p/W and Cu/W

	Pure W	ZrC_p/W	Cu/W
Density, $g \cdot cm^{-3}$	18.3	13.9	17.1
[a]Linear ablation rate, $\mu m \cdot s^{-1}$	12.6	2.74	9.4
[a]Mass ablation rate, $mg \cdot s^{-1}$	39.1	62.3	9.6
[b]Thermal diffusivity, $mm^2 \cdot K^{-1}$	34.8	13.5	47.1
[b]Thermal conductivity, $W \cdot m^{-1} \cdot K^{-1}$	99	39.1	135
Coefficient of thermal expansion, $10^{-6}K^{-1}$ (20–1000°C)	5.9	5.0	5.6
Hardness, Gpa	3.41	5.77	2.79
Flexural strength, MPa	–	705	483

[a]Data were tested after ablated for 120 s.
[b]Data were tested at 1000°C.

resistance and better mechanical properties such as flexural strength and hardness, comparison with Cu/W materials, make ZrC_p/W be suitable for the manufacture of the rudders for rocket motors instead of Cu/W.

4. Conclusion

As a result of the investigation of the effect of ZrC particles on the elevated temperature ablation resistance and thermalphysical properties for ZrC_p/W composites, the followings were found:

(1) The elevated temperature ablation resistance of the tungsten composites is remarkably increased with an addition of ZrC particles. The values of mass ablation rate of ZrC_p/W, pure W and Cu/W are in the order from low to high: ZrC_p/W < pure W < Cu/W, and the linear ablation rate are in the order: ZrC_p/W < Cu/W < pure W. ZrC_p/W possesses better ablation resistance than Cu/W.

(2) The addition of ZrC particles in tungsten matrix greatly decreased the thermal diffusivity and thermal conductivity of ZrC_p/W composites. The low thermal diffusivity and low thermal conductivity of ZrC_p/W can effectively prevent the outer heating flow diffusing into the inner of the materials, which resulting in a high temperature zone only existing in the surface zone of the materials, furthermore both of the melting points of ZrC and W are all very high, thereby, the elevated temperature ablation resistance of ZrC_p/W is significantly increased.

(3) The important temperature curves of the ablated surfaces of these specimens during eroding were detected online using a dynamic responding multi-wavelength pyrometer, which indicated that ZrC_p/W composites have good thermal shock resistance. Thermal thermochemical oxidation of tungsten matrix and ZrC particles is the main ablation mechanisms of ZrC_p/W composites.

(4) The higher strength, higher hardness, lower density, lower thermal conductivity and higher elevated temperature ablation resistance of ZrC_p/W compared with Cu/W makes ZrC_p/W be suitable for the rudders for rocket motor instead of Cu/W. Furthermore, there is no infiltrating copper procedure during the preparation of ZrC_p/W, implying a lower cost comparison with the preparation of Cu/W.

Acknowledgements

The authors would like to express their gratitude to Dr. Y. K. Guo for his help with the experiments. This project was supported by the China Postdoctoral Science Foundation and China National Distinguished Youth Science Foundation (No: 59725602).

References

1. S. W. H. YIH and C. T. WANG, "Tungsten-Sources, Metallurgy, Properties and Application" (Plenum Press, New York, 1979) p. 352.
2. Q. YU, "Materials Techniques" (Aerospace Press, Beijing, 1991) p. 7.
3. G. M. SONG, Y. ZHOU, Y. J. WANG and T. C. LEI, *J. Solid Rocket Technology* **21**(2) (1998) 51.
4. K. Q. MENG, K. Z. XU, A. B. WEI and G. L. XU, *J. Iron and Steel Research* **7**(5) (1995) 89.
5. G. M. SONG, Y. ZHOU, T. C. LEI and Y. J. WANG, *Aerospace Technology* **6** (1997) 43.
6. T. W. CLYNE and P. J. WITHNERS, "An Introduction to Metal Matrix Composites" (Cambridge University Press, New York, 1995) p. 1.
7. Z. Q. CHEN and S. Y. LI, *Science and Technology of Tungsten and Molybdenum* **3** (1983) 7.
8. G. M. SONG, Y. ZHOU and T. C. LEI, *J. Solid Rocket Technology* **20**(4) (1997) 53.
9. G. M. SONG and Y. ZHOU, *Aerospace Materials & Technology* **29**(1) (1999) 12.
10. T. Y. KOSOLAPOVA, "Handbook of High Temperature Compounds: Properties, Production, and Application" (Hemisphere Publication Corporation, New York, 1990).
11. G. M. SONG, Y. ZHOU, Y. J. WANG and T. C. LEI, *J. Mater. Sci. Lett.* **17** (1998) 1739.
12. G. M. SONG, Y. P. YANG, Y. ZHOU, Y. J. WANG, Y. K. GUO and T. C. LEI, *Mining and Metallurgy* **9**(3) (2000) 76.
13. L. ZHANG and J. XUE, *Ref. Metal & Hard Mater.* **9** (1990) 167.
14. T. G. XI, "Thermophysical Properties of Inorganic Materials" (Shanghai Science and Technology Press, Shanghai, 1981) p. 208.
15. S. M. YANG, "Heat transfer" (High Education Press, Beijing, 1987).
16. Z. A. GUO and K. H. WANG, "Spray Painting and Cladding of Alloying Powders using Oxyacetylene Flame" (Coal Industry Press, Beijing, 1985) p. 112.
17. S. F. PENG, "Metallurgy of Tungsten" (Metallurgy Industry Press, Beijing, 1981) p. 168.

Received 17 October 2000
and accepted 14 May 2001